A curved crystal spectrometer for energy calibration and spectral characterization of mammographic x-ray sources

Lawrence T. Hudson, Richard D. Deslattes, Albert Henins, Christopher T. Chantler,[a)]
Ernest G. Kessler, and John E. Schweppe
National Institute of Standards and Technology, Gaithersburg, Maryland 20899

(Received 28 December 1995; accepted for publication 24 June 1996)

Clinical efficacy of diagnostic radiology for mammographic examinations is critically dependent on source characteristics, detection efficiency, image resolution and applied high voltage. In this report we focus on means for evaluation of source-dependent issues including noninvasive determination of the applied high voltage, and characterization of intrinsic spectral distributions which in turn reflect the effects of added filtration and target and window contamination. It is shown that a particular form of x-ray curved crystal spectrometry with electronic imaging can serve to determine all relevant parameters within the confines of a standard clinical exposure. © *1996 American Association of Physicists in Medicine.*

Key words: curved crystal spectrometry, diffraction, high voltage, mammography, x-rays

I. INTRODUCTION

Current technical and regulatory activities directed toward improved mammographic image quality respond to both the problem's urgency and its technical difficulties. Among the several requirements for procedural and parametric standardization,[1] operating conditions and spectral output of the x-ray source are most amenable to simple metrological procedures. The control of patient exposure is primarily a dosimetric consideration and not further addressed here. This report undertakes the remaining source related issues, viz., determination of applied high voltage and verification of the assumed spectral distribution.

Particularly for film-screen mammography, image quality has been shown to be sensitive to changes in the applied high voltage (HV) as small as 1 kV[2,3] in the customary mammographic range of 22 kV to 40 kV. To assure delivery of such a performance in the clinical environment, kVp measuring procedures must have smaller uncertainties than 1 kV. Calibrations derived from national standardizing laboratory procedures would require still smaller errors, perhaps near 0.3 kV. (This "rule of three" is often applied in this laboratory; it is the factor between the accuracy realized at the primary standards laboratory and that needed in the field.) Although traditional, "invasive" (with respect to the power source) high-voltage divider technique offers adequate accuracy for the case of well-filtered DC potentials, problems arise from the limited accessibility of HV test points in modern generators and from the HV ripple. Since this ripple can vary from a few times power line frequencies to over 100 kHz, broad band frequency compensated dividers are required whose calibration is not easily assured.[4] These difficulties have prompted development and application of several noninvasive alternatives as briefly described in the following paragraph.

The principal noninvasive techniques in fairly widespread use at the present time include differential x-ray filter methods,[5–7] which are particularly convenient for testing clinical installations, ionization spectrometry, which is more frequently applied in standardizing laboratories,[8,9] and Compton scattering spectrometry.[10–12] Although the latter two methods offer high accuracy (*ca.* 0.2 kV) and are readily calibrated with respect to radioactive sources or x-ray emission line standards, acquiring the needed spectral data during the interval of a standard clinical exposure is somewhat difficult owing to the time required for event-by-event photon counting. Procedures using differential filters offer greater simplicity, convenience, and are less expensive relative to the other two methods. Differential filter methods that use two thicknesses of the same element have a wider range of application but a more slowly varying response to HV changes[13–16] as compared to methods using absorbers with a critical threshold in the range of interest. Both of these filtration methods, however, require some calibration since the response functions are sensitive to target material, intrinsic filtration, and electrical waveform. [High performance differential filter kVp meters generally require separate calibration settings according to anode type, filtration, and (less frequently) high voltage waveform.] A less widely used variant of the critical filter method, developed at the National Physical Laboratory (NPL) in the UK, is based on detection of fluorescent x-rays from the absorber.[17]

To overcome the limitations of the methods indicated above, we investigated the application of crystal diffraction spectrometry to the problem of HV measurement and spectral characterization. The first report of this work[18] describes an adaptation of a symmetric, transmission geometry (Laue-case) flat crystal diffraction spectrograph[19,20] to these problems. As is the case with all noninvasive techniques, it is based upon the conservation of energy: Bremsstrahlung or continuum radiation is produced by an x-ray tube with energies up to a high-energy cutoff; this "endpoint" energy of the spectrum is produced by electrons which have fallen through a potential difference of HV and given up all their energy as a photon.

 0094-2405/96/23(10)/1659/12/$10.00

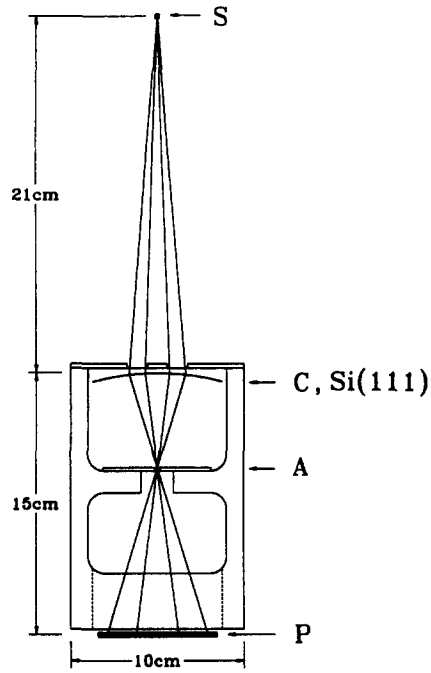

FIG. 1. Diagram of a curved-crystal spectrometer for energy calibration and spectral characterization of mammographic x-ray sources. X-rays originate at source S, are diffracted by crystal C through aperture A and are imaged at plane P. The dimensions shown are appropriate for use with a Si(111) crystal bent to a 15 cm radius of curvature.

The initial prototype spectrograph used photographic registration and suffered from the source-size dependent resolution intrinsic to imaging by flat crystal x-ray optics. In the present communication we describe a second generation instrument in which a curved crystal optic provides improved efficiency and gives spectroscopic resolution independent of source size.[21] The new instrumentation uses a charge coupled device (CCD) dental imager permitting convenient electronic registration of the spectrum and its prompt presentation on a computer screen. These developments allow full spectral characterization of mammographic sources and HV calibration to be realized within the parameters of standard mammographic exposures. Results presented on the computer display are immediately accessible to fitting routines which yield the applied HV. Calibration markers, included in the spectral data either through target lines or added absorbers, permit self-standardization of field instruments. This method of standardization avoids the progressive loss of accuracy inherent to conventional hierarchical calibration modalities.

II. GEOMETRY OF A CURVED CRYSTAL DIFFRACTION SPECTROMETER

Limitations of the previous flat crystal instrument are largely overcome by the geometry of the current instrument which is illustrated in Figure 1. X-rays from the source, S, are dispersed and focussed by the curved crystal, C, and proceed through a central, background-suppressing aperture, A, onto a fixed image plane, P. This geometry is a modification and extension of that proposed by Cauchois in 1932;[22] rather than a single spectrum, two mirror-symmetric spectra are imaged as was the case with the previous flat-crystal spectrometer. Not only does this curved-crystal geometry provide insensitivity to focal spot size, but it also enhances spectral dispersion and, because of the focusing action of the bent crystal, increases the efficiency of the spectrometer. In the current prototype, the image is captured by a phosphor sensitized charge coupled device (CCD). This sensor is discussed in more detail in Section III. The spectrometer dimensions shown in Figure 1 pertain to the case of a Si(111) crystal (inter-planar spacing 0.314 nm) curved to a radius of 15 cm. A more extended treatment of such instruments is given in a companion publication.[23]

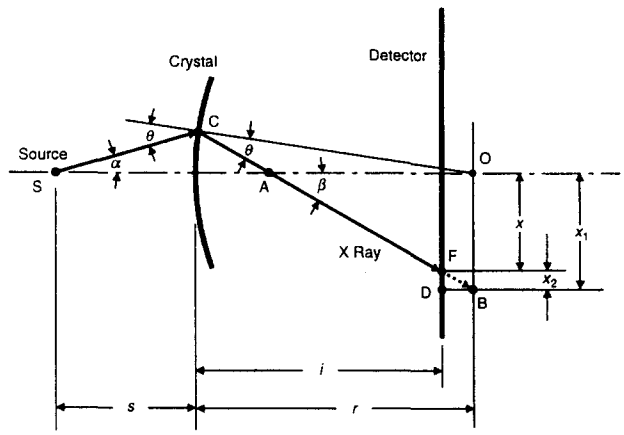

FIG. 2. Schematic showing the geometry of the source, crystal, and detector used in derivation of the curved crystal spectrometer dispersion function. In particular, s is the distance from the source to crystal center, i is the distance from crystal center to detector, and r is the radius of curvature of the crystal.

The dispersion function for a spectrographic instrument is the relation between the transverse coordinate in the spectrometer's image plane and the energy (or wavelength) of the x-rays registered at that position. While this function has a very simple form for the flat crystal geometry,[18] the present curved-crystal geometry entails greater complexity. The derivation which follows assumes ideal alignment of source, crystal, scatter baffle, and plane of detection (effects of misalignment are discussed in Ref. 23). As shown in Figure 2, the crystal has a radius of curvature r, the imaging detector is located a distance i away from the crystal and the source is located a distance s away from the crystal along a perpendicular to the detector. For this derivation, consider x-ray emission only in the plane of the figure; large out-of-plane diffraction would result in curved spectral "lines," but this is not evident in the images acquired with the spectrometers described here. The ray path indicated leaves the source and is diffracted by the crystal at a Bragg angle θ, and impinges on the detector plane at the distance x from the spectrometer centerline. Since symmetric Laue case diffraction is not encumbered by an index of refraction correction, the diffraction angle, θ, is simply related to x-ray wavelength, λ, and energy, E, through $\lambda = (2d/n)\sin\theta$ and $E = hc/\lambda$ with $hc = 1.9864475 \times 10^{-25}$ J·m(1.23984244 nm·keV)[24] where d

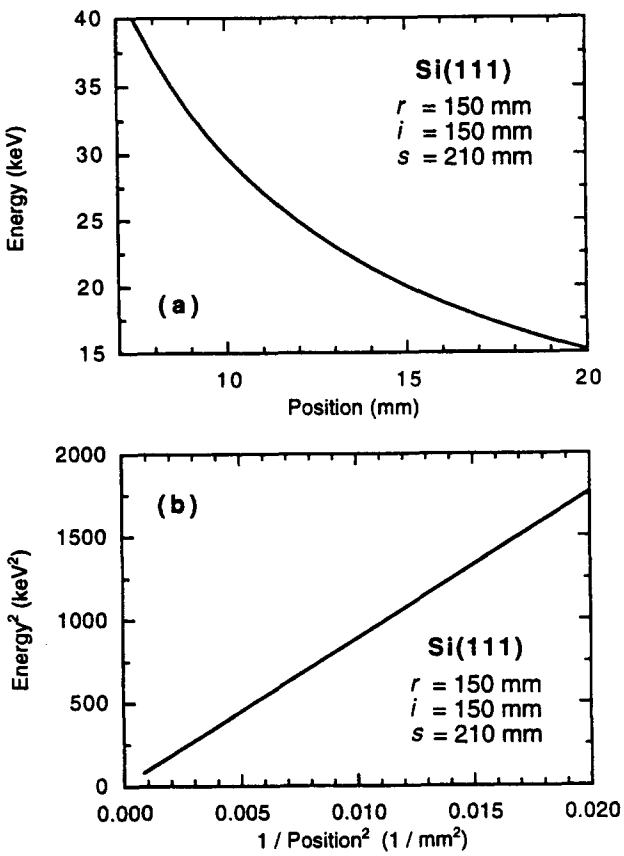

FIG. 3. (a) Calculated dispersion function for the curved crystal spectrometer shown in Figure 1. (b) Data of (a) replotted against a new set of variables.

is the lattice spacing of the crystal, n is the order of diffraction. $n=1$ in the cases considered here.

The dispersion function derivation is simplified by introducing a new parameter, u, which is functionally related to the Bragg angle through $u=\sin\theta$. In terms of this new parameter, a series of geometrical relationships (given in Appendix A) can be arranged to give

$$x(E)=[r+(i-r)v]\frac{u}{w},$$

where

$$v\equiv 2\sqrt{1-u^2}\sqrt{1-f^2u^2}-f(1-2u^2),$$

$$w\equiv(1-2u^2)\sqrt{1-f^2u^2}+2fu^2\sqrt{1-u^2},$$

$$f\equiv r/(r+s),\quad u=E_0/E,\quad E_0\equiv nhc/2d.$$

In practice, one is interested in $E(x)$, in which case the equation shown above can be numerically inverted. This inversion is easily addressed in the numerical algorithms which would be used for extracting spectral distributions and endpoint energies. In the special case where $r=i$, it is then possible to express $E(x)$ parametrically or as an unwieldy analytic expression. An example of this dispersion function is shown in Figure 3(a) for the spectrometer shown in Figure 1. Here the Si(111) planes are used in first order with $d=0.3136$ nm, $r=i=150$ mm, and with the source placed $s=210$ mm from the crystal. It is clear from Figure 3(a) that the number of pixels/kV decreases along the detector as one approaches, from either direction, the centerpoint of the two spectra—which itself is at zero wavelength or infinite energy. The simple behavior of the dispersion curve in Figure 3(a) invites use of empirical approximations over limited energy ranges. For example, the expression $E^2=a/x^2+b$ can replace the exact, inverted dispersion relation $E=E(x)$ with an imprecision of less than 1 eV over the range of energies used in mammography. [We are indebted to J. H. Marshall, Radcal Corporation, Monrovia, CA for pointing out this particular form for approximating the dispersion relation. This form is discussed further in Appendix A.] In Figure 3(b), the data of Fig. 3(a) are replotted as E^2 versus x^{-2} to suggest application of a linear approximation.

III. IMAGE REGISTRATION AND ANALYSIS

A. Electronic registration of spectral images

Photographic registration of spectral data, as used in our earliest flat and curved crystal prototype spectrometers, entailed an inconvenient delay for film development and densitometry, and the background noise was a limiting factor. Our recent efforts have accordingly emphasized use of electronic imaging technology interfaced to a portable computer in order to make possible immediate analysis in the field. While any of the several available approaches to direct electronic x-ray imaging would suffice, cost-effectiveness considerations led to the choice of large-area digital radiography sensors developed as replacements for dental films. [The particular sensor in use at the present time was obtained from the Schick Technologies, Inc. The identification of a particular commercial products here and elsewhere is not intended to indicate uniqueness, or particular suitability to the application described.] This sensor is a charge coupled device with an active area of 36.5 mm ×25.2 mm; it has an array of 760× 524 square pixels each 48 μm on a side. It is packaged in an aluminum case as a 6 mm thick sandwich consisting of a scintillator, which converts x-rays to visible light, fiber optic faceplate, CCD, and I/O cable. The sensor and power supply are connected in turn to a PC-based ISA bus interface card. (The acronyms PC and ISA refer to a widely used personal computer architecture and its associated data bus specification, respectively.) Available software captures 12-bit images for a user-specified amount of time at a spatial resolution of 9 to 10 line pairs per millimeter. A biasing scheme suppresses the dark current and allows extended exposures without requiring active cooling.[25,26]

B. A pinhole camera along spectrometer centerline

The long-term integrity of the focal spot size and shape is also an important diagnostic radiological parameter.[27] It can easily be monitored in the present instrument by introducing a pinhole camera along the center axis of the spectrometer. When the spectrometer is centered in the central beam of the x-ray source, the focal spot is imaged in the center of the CCD, a pixel area which is not otherwise being used. We

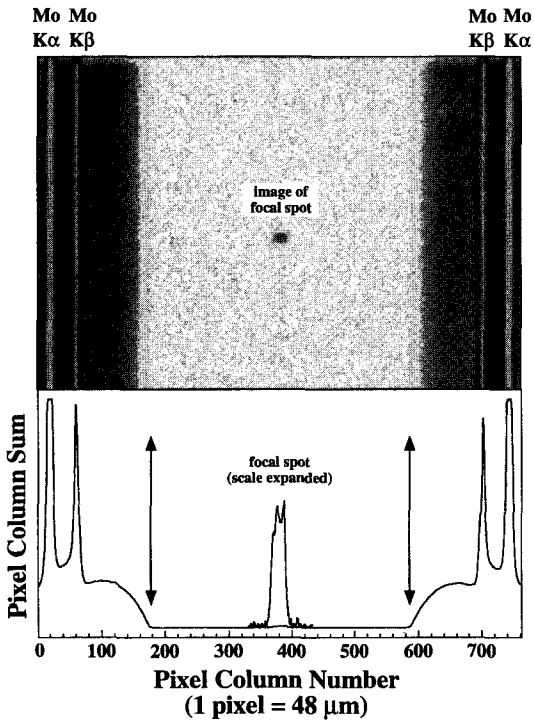

FIG. 4. Top: Grayscale image from a quartz-crystal spectrometer acquired with the dental CCD described in the text. A pinhole-camera image of the focal spot is visible in the center of the image. Bottom: The pixel column sum plot or spectrum of the image shown above. This shows the molybdenum spectrum (the alpha lines are saturated) and the image of the focal spot in the center. The high-energy cutoff of the spectrum is marked by the arrows.

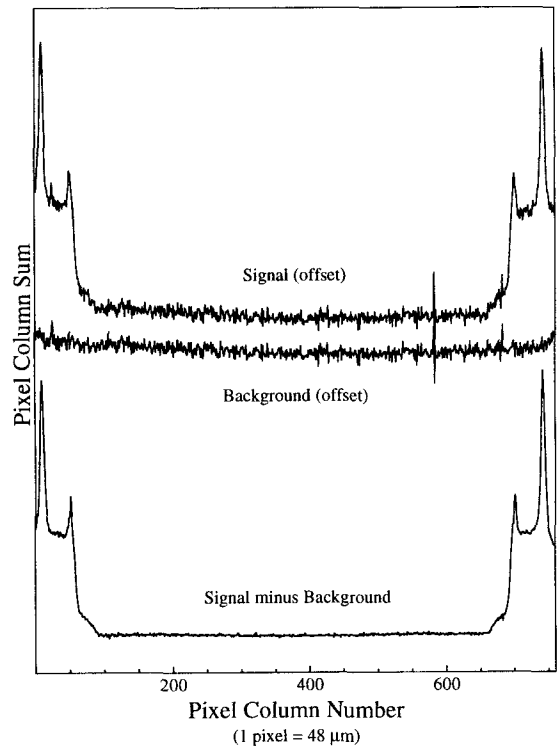

FIG. 5. Demonstration of the effectiveness of dark-current image subtraction to reduce fixed pattern noise. This is a long-duration exposure (54 s) and therefore an extreme example.

have found that a pinhole of about 30 μm diameter permits satisfactory imaging without saturating the CCD.

The top portion of Figure 4 shows a two-dimensional grayscale image acquired with a quartz-crystal spectrometer using the digital sensor and a laboratory x-ray source. The image was acquired with an exposure of 11 mAs and a background or "dark current" image has been subtracted; this is discussed in section III C. The spectrometer used a 230 μm thick Qz ($10\bar{1}1$) crystal (47 mm by 27.5 mm) which was bent along its long axis to a radius of 16.5 cm. In the center, one sees the structure of the focal spot of the x-ray source imaged by the pinhole camera. The pinhole is in the center of the faceplate and, in this camera, was somewhat larger than 30 μm. A 1 mm-thick aluminum attenuator was placed in front of the pinhole to prevent sensor saturation from obscuring the structure within the focal spot image. The pixel column summed profile of this image is shown at the bottom of Figure 4; the Mo Ka lines have saturated the sensor. The endpoint energy of the continuous x-ray spectrum (indicated by the arrows) is 30 keV and numerically equal to the 30 kV high voltage through which electrons have been accelerated in the source.

C. Subtraction of fixed pattern noise from CCD images

A background image is one acquired with the same integration time but with no x-ray exposure, generally immediately before or after acquiring an x-ray image. Pixel by pixel subtraction of this dark image greatly reduces the effect of fixed pattern noise leaving only dark-current shot noise in each pixel. (This quantum noise can be reduced further by averaging several background images.) This benefit derives from the short-term reproducibility of thermal accumulation of charge by "hotter" than average pixels (dark spikes) due to lattice faults or impurities in the sensor material. The efficacy of this procedure is illustrated in Figure 5 which shows the pixel column sums of the two exposures along with the pixel column sum of the difference image. This spectrum was taken with a 180 μm focal spot Mo x-ray source at a potential of 22 kV, exposure of 134 mAs, and with 25 μm of added Mo filtration. The spectrometer used a Si(111) crystal bent to $r = 15$ cm which had undergone the surface-abrasive treatment described in Appendix B and a CCD sensor which had been retrofitted with a higher sensitivity intensifying screen (Section IV). The accumulation time in this demonstration exposure is much longer than would be needed in a clinical setting where the sources operate at much higher current levels yielding images in much shorter typical integration times. One can also see from the figure that this analysis can largely remove artifacts due to pixel, and to some extent, column defects which are inherent in the CCD.

D. Reducing the dynamic range of incident spectra

The x-ray spectra emitted from mammographic sources may include high-intensity characteristic target lines as well

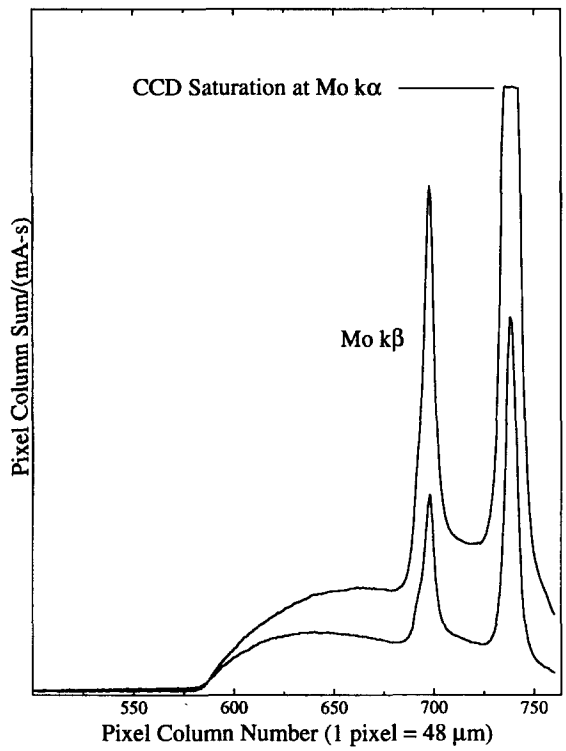

FIG. 6. Demonstration of the compression of the dynamic range of the incoming spectrum using a 1.3 mm glass attenuator.

as the very low-intensity region near the high-energy cutoff or endpoint of the spectrum. To obtain good statistics in the spectrum near the high-energy cutoff without saturating on the characteristic lines requires either a detector with a large dynamic range or a means of compressing the dynamic range the imaging detector must record. Should this be desired, such a compression is conveniently and economically accomplished by introducing an attenuator of appropriate thickness and composition to preferentially reduce lower energy photons x-rays. This could, for example, suppress the intense characteristic emission lines from Mo or Rh sources while passing relatively more intensity in the higher-energy endpoint region of the spectrum. Generally a low-Z attenuator would be chosen so as to avoid absorption edges in the spectral region of interest. For low energy studies where absorption of the dimmer spectral features becomes significant, it might be appropriate to mask only that portion of the detector illuminated by the brightest spectral features. Figure 6 shows the effect of a 1.3 mm glass microscope slide in reducing the dynamic range of a recorded spectrum. The attenuator was placed at the entrance aperture of a prototype spectrometer using a Qz $(10\bar{1}1)$ analyzing crystal (the selection of an optimum crystal is discussed in Section IV) and a CCD dental sensor retrofitted with a gadolinium oxysulfide (Gd_2O_2S) scintillating screen which was 150 μm thick. (This type of screen is manufactured for use in film screen mammography and is commercially available from Eastman Kodak under the designation "Lanex regular .") Both spectra were acquired using 15 mAs at an applied voltage of 30 kV. As shown for the nonattenuated spectrum, the Mo Kα doublet saturates the full-well capacity of the CCD. With the glass attenuator, the dynamic range of the input spectrum has been effectively compressed. While available intensities are much greater in clinical installations, their often unremovable filtration tends to offset this gain in intensity. When spectral profile information is of interest, the analysis software will have to correct for the transmission of an attenuator if one is used. These energy-dependent attenuation functions are well known.[28]

IV. OPTIMIZATION OF OVERALL SYSTEM PERFORMANCE

Early versions of the curved crystal instrument used Si(111) crystals and unmodified dental CCD sensors. These produced good results but required relatively extended exposures under laboratory conditions. To realize the sensitivity needed to register spectral data of adequate quality within the parameters of a single exposure of a clinical mammographic source required improvements in both detector and crystal performance. In part, this need for increased sensitivity was driven by source attenuation due to added filtration found in many mammographic sources and the occasional difficulty in effecting its removal. Additionally, it is sometimes desirable to characterize source spectra including the effect of added filtration.

A. Modifications of detector electronics and phosphor converter

In its original form, the dental CCD detector was not well matched to the requirements of this application. The sensitivity shortfall arises not only from the smaller photon flux levels available but also reflects the fact that the mammographic energy region (22–40 keV) lies below the dental x-ray region (40–70 keV). We have undertaken several measures to gain the required sensitivity. Some sensitivity improvement was realized by increasing video amplifier gain prior to the signal digitization. The gain increase of approximately fivefold was chosen to produce a modest level of "fogging" or thermal background growth after several seconds of integration time.

A second step toward gaining higher sensitivity, albeit at some cost in resolution, involved substituting a high sensitivity phosphor screen for the normal thinner directly applied phosphor converter. The higher sensitivity x-ray intensifying screen used was a 150 μm-thick converter of doped Gd_2O_2S. The sensitivity increase obtained through this change was a factor of 4 $\pm$ 5% over the energy range used in mammography. This substitution had the unwelcome but tolerable effect of reducing the spatial resolution of the sensor from 9 to 10 line pairs per millimeter (lp/mm) to about 6 lp/mm.

B. Choice and preparation of diffraction crystals

The range of crystals and diffraction planes which might be used in the present application is constrained by several technical considerations. Among these constraints, the size range of economically acceptable imagers and the working

distance limitation to the focal spot are the most obvious. The alternative crystals examined and their relative performance parameters are summarized in Appendix B. The current crystal of choice is natural quartz (Qz) with the $(10\overline{1}1)$ planes active. This material is readily available and plates sufficiently thick (about 0.25 mm) for efficient diffraction are elastically bendable to the needed radius (15 cm). In comparison with the results obtained initially from Si(111) (thickness 0.185 mm), the transmitted intensity is larger by a factor of about eight due primarily to the elastic (quasimosaic) Sumbaev effect[29] in quartz as discussed in Appendix B. In combination with the modified detector, the system sensitivity is more than a factor of thirty greater than our initial curved-crystal prototype (not counting the increase in the electronic gain). As a consequence, spectra from filtered sources can now be easily registered within the exposure time of a normal mammographic exposure. This is true for the unmodified, higher-resolution CCD sensor except under conditions of low kV and heavy filtration.

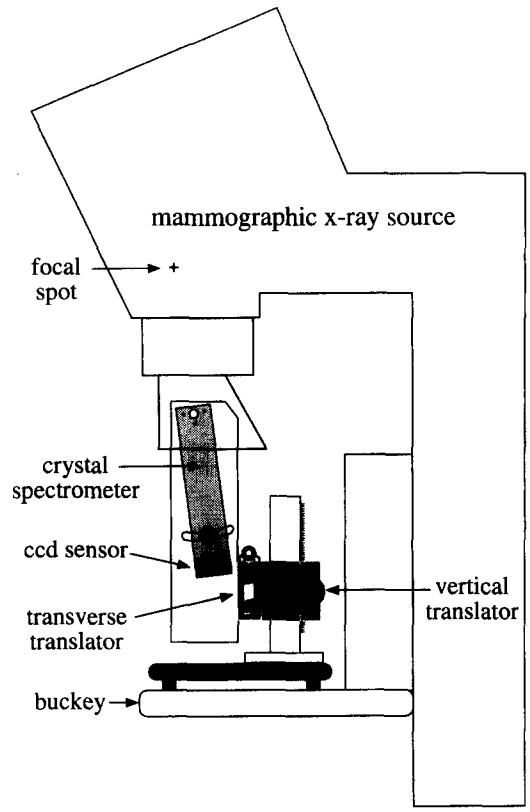

FIG. 7. Schematic of spectrometer and positioning system with a clinical mammographic x-ray source.

V. PRELIMINARY RESULTS

A. Portability and alignment protocol

Efforts have also been directed toward realizing more convenient packaging, enhanced portability, and ease of installation and use. The present system consists of a low-cost notebook computer with a single, internal ISA bus which holds the CCD interface card. This fits conveniently in a normal size briefcase with the interface power supply, calibration foils, and some small tools. The spectrometer itself is mounted with three degrees of freedom as illustrated schematically in Figure 7. After it is placed on a standard mammographic platform, its height is adjusted with a vertical translation stage to the nominal working distance of 20 cm from the focal spot. The kV results are relatively insensitive to this parameter and the needed accuracy of a few centimeters is obtained with a measuring tape. Gross spectrometer positioning is aided by viewing the shadow pattern of the entrance baffle on the sensor package using the field illumination lamp available in most mammographic systems. This image is visible because of the transparency of both the quartz analyzing crystal and the lead acrylic top of the spectrometer body. Final alignment is done with x-rays. We have performed initial testing of this prototype spectrometer with a variety of clinical sources. Set up and alignment generally took about ten minutes. On occasion, adequate alignment was more elusive. In such cases, time could be saved with the use of interchangeable pinholes of various sizes and a retractable crossover slit. Fine lateral tuning is accomplished by a screw-driven adjustment in the plane of dispersion to center the image of the focal spot between the two mirror-image x-ray spectra. This is done iteratively by adjusting the position between test exposures until centering is achieved to within a few tenths of a millimeter. Finally, the spectrometer's supporting cradle allows its plane of dispersion to be tilted with respect to the vertical so as to accommodate different anode orientations. When either a different anode track or filament is used, some fine repositioning may be needed to re-center the image on the sensor.

B. Spectral results

Preliminary results have been obtained using several laboratory x-ray sources with Mo anodes and at a few clinical sites. [In house laboratory work used a compact microfocus source of a type available for magnification mammography (Tru-Focus MXT 7100 Moly x-ray tube with 0.15 mm focal spot) or a Ge-CA8L Mo tube with nominal focal spot of 1.3 mm.] The data discussed in this section were obtained using a quartz crystal spectrometer with modified sensor head and sensor electronics. A group of spectra illustrative of what would be obtained in a clinical calibration sequence is shown in Figure 8. These spectra are from a source with no intrinsic filtration, however the spectra are modified by addition of a 1 mm Al filter to reduce the range of intensities applied to the imaging detector. In practice, such spectra would more likely be obtained at intervals of 1 kV rather than at the 5 kV intervals indicated. These particular spectra were obtained in a laboratory environment with a small focus source and a low ripple HV supply and normalized to a common exposure; each was acquired with less than 60 mAs. The formalism developed in Appendix A has been applied to extract the endpoint energy of spectra acquired in the laboratory and in the field; the results are discussed below in Section V C.

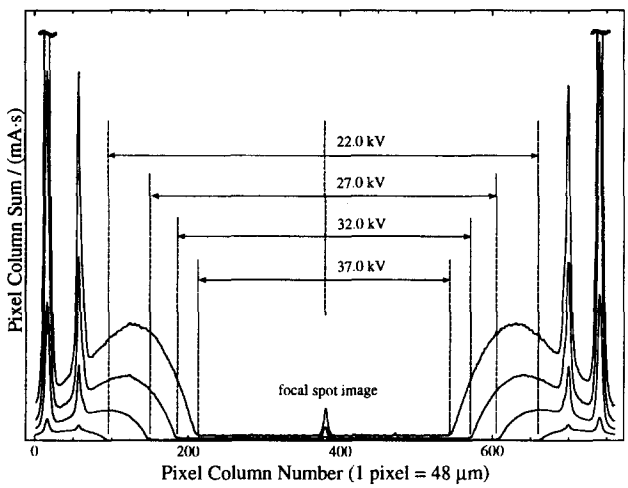

FIG. 8. Series of calibration spectra at different energies filtered with 1 mm of aluminum.

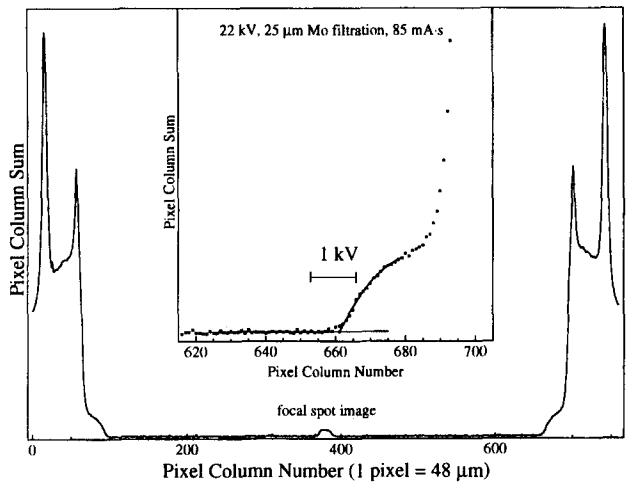

FIG. 10. Low intensity spectrum acquired at 22 kV, 25 μm Mo filtration, and 85 mAs exposure.

Installations having large amounts of HV ripple will give spectra whose endpoint profiles are less sharply delineated. On the other hand, the associated spectra accurately portray the time-averaged radiation profile used.

To indicate the effects of filtration commonly used in clinical applications, data were acquired with a 25 μm molybdenum filter and a 1 mm aluminum filter. Figure 9 shows these spectra on a logarithmic scale normalized to exposure. Note that the continuum radiation is most suppressed by the Mo filter while the Mo Kα source lines are more suppressed by the Al filter. Filtering with a microscope slide (1.3 mm glass) produces an almost identical spectrum in the region of the Mo K radiations to that produced by 1 mm of aluminum.

Figure 10 illustrates the overall spectrometer system sensitivity in what may be considered a nearly "worst case" situation. The spectra were obtained at the (rather low) HV level of 22 kV with a 25 μm Mo filter and only 85 mAs. The inset graph shows the region of the endpoint energy and the scale of 1 kV in this energy region (thirteen pixels).

This technique is extensible to the higher energies used in diagnostic radiography aside from mammography. To ac-

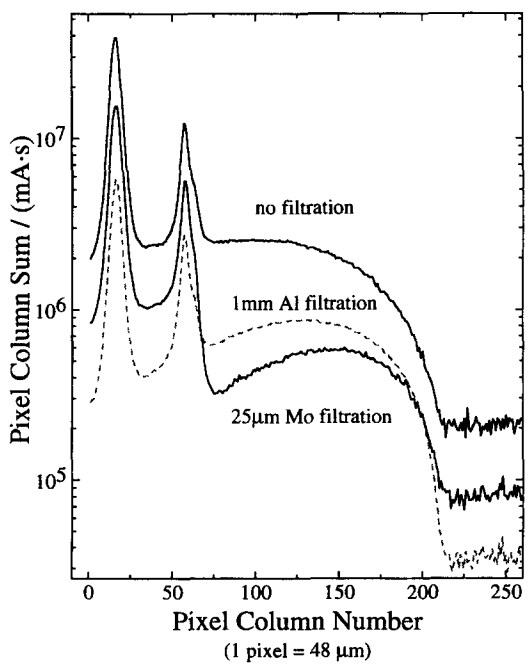

FIG. 9. Demonstration of the effects on the output spectral distributions due to commonly used filter materials.

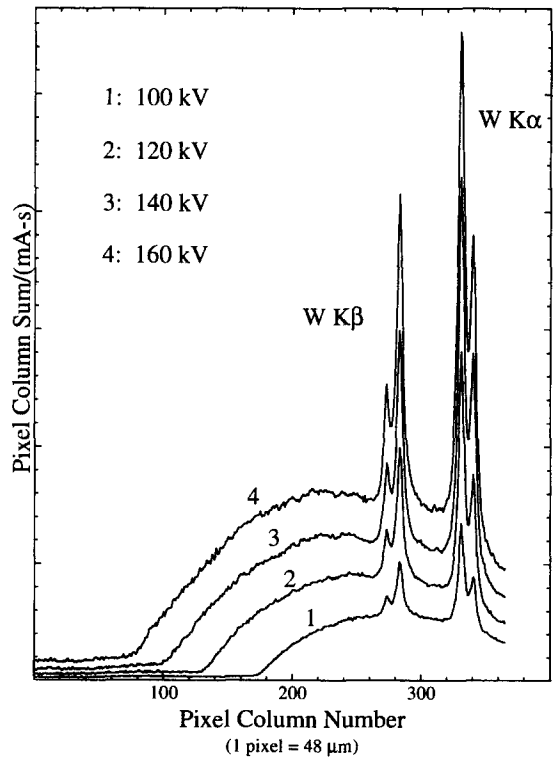

FIG. 11. High-energy spectra (100 to 160 keV) acquired with the dental CCD described in the text.

commodate the smaller Bragg angles associated with these higher energies, we used an extended version of the spectrometer shown in Figure 1 which was configured for a source to crystal distance of 1120 mm and a crystal to image plane distance of 370 mm. High-energy spectra were obtained using the (220) diffracting planes of a germanium crystal bent to a radius of 370 mm and x-ray sensitive film. The tungsten anode source used had a 3.8 mm ×3.8 mm focal spot and 7 mm Be window; an attenuator of 0.25 mm of Mo was added to reduce the dynamic range of the spectra. In this preliminary work, no attempt was made to match the full spectral image pattern (width 45 mm) with the size of the available dental CCD (width = 37.5 mm) so that we registered only one of the two mirror-symmetric spectra as shown in Figure 11 for applied x-ray voltages in the range of 100 to 160 kV. The spectra show the W K-alpha (59 keV) and K-beta (67 keV) emissions and a high-energy cutoff of the continuum radiation with an acceptable ratio of signal to noise. Background images were subtracted before generating the pixel column sums. Each of the spectra was acquired with 10 mA source current and have been normalized to exposure time. The 100 kV spectrum was acquired with about 650 mAs; 120 kV, 350 mAs; 140 kV, 270 mAs; 160 kV, 230 mAs. These exposures can be reduced by optimizing the screen thickness for higher energies.

C. Initial performance estimates

Analysis of spectra acquired with a flat crystal spectrometer is particularly simple:[18] the location of a single spectral feature pair is sufficient to calibrate the instrument to extract the voltage applied to the x-ray source. The formalism derived in Appendix A [Equations (A10) and (A11)] shows that, in contrast with the flat-crystal case, a curved crystal spectrometer has four independent parameters in a nonlinear dispersion function relating lateral image displacement from the center of the detector to energy: r, d, i, and s; a fifth parameter, detector pixel size, is needed to relate pixel number to actual displacement. To calibrate such a camera, one could, in principle, measure each of these geometrical parameters with attention to their respective sensitivities. (For example, an uncertainty in the radius of curvature of the crystal of 0.5 mm introduces an uncertainty of 0.1 keV in the endpoint energy at a voltage of 32 kV.) Any or all of these geometrical measurements may be eliminated by using an equal number of spectral markers of known energy, including characteristic spectral lines from the anode and absorption edges. The edges can be easily superimposed on a spectrum by placing thin foils between the source and the spectrometer.

However, as further shown in Appendix A, curved-crystal-spectrometer calibration can be much simpler, indeed comparable to the case of the flat-crystal spectrometer. The exact, nonlinear dispersion relation connecting E to x can be replaced by a simpler, linear relation between E^2 and x^{-2},

$$E^2=\frac{a}{x^2}+b,$$

to an accuracy of better than 1 eV over the range of energies and spectrometer configurations of interest to mammographic calibration. The two coefficients, a and b, of this linear approximation of the dispersion function can be determined from the geometrical parameters of the spectrometer, as derived in Appendix A, or, perhaps more practically, from a calibration involving at least two spectral features of known energy.

To obtain an initial estimate of the absolute accuracy that might be obtained using the technology described in this report, we first calibrated the detector scale of a spectrometer with the approximation shown above with the positions of the K-edge of thin foils of tin, cadmium, silver, and palladium. Operationally, "positions" are defined as half the distance between identical features of the left and right recorded spectra; this tends to reduce errors due to imperfect alignment of source, crystal, and detector in the plane of dispersion. The residuals due to fitting the dispersion function to the foil edges were all less than 0.02 kV. We then used this calibration to determine the endpoint energies of a series of spectra (such as shown in Figure 8) recorded at six voltages between 22 kV and 36 kV. Endpoint positions were determined by fitting to the region of the endpoint to a function that is linear above the endpoint energy and cubic below the endpoint. We compared these extracted endpoint energies with concurrent measurements of a voltage divider connected to our laboratory x-ray source supply. The step-down resistor was itself calibrated at NIST in the Electrical Engineering Laboratory. Careful application of this methodology provided agreements to within 0.1 kV. The uncertainty in this scheme is dominated by uncertainties in the determination of the endpoint locations and in the calibration of the voltage divider rather than any intrinsic property of the spectrometer itself. We estimate that this level of accuracy could be significantly improved by more sophisticated modeling of the high-energy endpoint region and edge transmission function and by higher resolution image registration.

We also note that for some clinical sources tested, scattered radiation could contribute a nonuniform background to the spectrum which in turn increases the uncertainty with which the endpoint energy can be extracted. It was found that a transverse pre-aperture either attached to the source side of the spectrometer or somehow otherwise inserted between the source and spectrometer could block this radiation which is scattered from the walls of the source and transmitted through aperture A of Figure 1 without being diffracted.

VI. CONCLUSIONS AND OUTLOOK

We have described the design principles and presented first results from a new curved crystal spectrograph which may be used to calibrate the high voltage applied to x-ray tubes used in mammography and determine the spectral distribution of the radiation produced. The overall system efficiency has been significantly enhanced from early prototypes[18] to now allow acquisition of full spectral data within the parameters of a standard clinical exposure. The technique is easily adaptable to the clinical setting.

By choice of lattice spacings and/or spectrometer dimensions, this spectrographic technique is also extensible to energy regimes both lower and higher than that employed in mammography. An example has been given (results shown in Figure 11) which shows spectra with endpoint energies up to 160 kV acquired with the dental CCD. Image quality in higher-energy radiological applications is less sensitive to applied source potential. These applications, however, do depend upon HV stability and reproducibility. This is because dosimeters used to standardize exposure employ gas ionization by x-rays which is a strongly varying function of incident photon energy. Extension to lower energies were of interest for the modeling of continuum spectra. We have built a working prototype spectrometer which registers spectra down to 12 kV. It employs a more transparent CCD faceplate (0.5 mm of lucite), a relatively thin x-ray converter, and the use of the $(10\bar{1}0)$ planes of quartz which have a lattice spacing of 0.426 nm. The quartz crystal was about 280 μm thick and bent to a radius of curvature of 145 cm to match the image width to that of the sensor.

The acquisition of full spectral information facilitates studies of new target and filter combinations, and possible changes in the output distribution due to tube aging. Specifically, there are two main issues that are easily accessible: (i) The full spectral characterization of test systems including conventional and novel x-ray sources with an extended range of filtration options will lead to either improved technique outside of the presently considered parameter space or to an appreciation that the present range of source and filter combinations is already optimal. (ii) Spectra produced in the cohort of x-ray tubes currently in clinical use may not be adequately represented by their nominal anode composition at the time of manufacture. If this spectral variability is encountered, then it will be of considerable interest to determine the extent to which these changes influence diagnostic efficacy at the level of phantom-based scoring procedures.

ACKNOWLEDGMENTS

Our early efforts toward the present instrumentation were encouraged and facilitated by R. Jennings and P. Quinn of CDRH and B. Coursey of NIST. We appreciate the assistance of Hamid Jafroudi of the Imaging Science and Information Science Systems (ISIS) Center, Department of Radiology, Georgetown University Medical Center. Current applications of the technology are proceeding in cooperation with John Boone, University of California, Davis, and Gary Barnes, University of Alabama, Birmingham. We are also indebted to Jochen Schneider (DESY, Hamburg) for supplying heavily oxygen-doped heat treated Si crystals, Martin Misakian (NIST) for calibrating our step-down resistor, and John Worthington (NIST) for expert machining. The work is supported by the U.S. Army's Breast Cancer Research Program (MIPR No. M4539FU6) and by NIST.

APPENDIX A: DERIVATION OF THE CURVED-CRYSTAL SPECTRAL DISPERSION FUNCTION

In this appendix, we give a more detailed derivation of the dispersion function for a spectrometer using the modified Cauchois geometry. As stated in the text, we assume ideal alignment of source, crystal, scatter baffle, and plane of detection. As shown in Figure 2, the crystal has a radius of curvature r, the imaging detector is located a distance i away from the crystal, and the source is located a distance s away from the crystal along a perpendicular to the detector. Consider x-ray emission only in the plane of the figure, i.e., assume the crystal has zero height. Let α be the emission angle of the x-ray from the source with respect to the perpendicular from the detector. The Bragg angle, θ, at which the x-ray is diffracted by the crystal is also indicated. X-rays impinge on the detector plane at an angle β as shown in the figure. The distance from the center of the detector to the point of detection of the x-ray is

$$x = x_1 - x_2. \tag{A1}$$

Consideration of the triangle BDF in Figure 2 shows that

$$x_2 = (r-i)\tan\beta. \tag{A2}$$

Applying the law of sines to the triangle COB with the angles θ and $(\pi/2-\beta)$ opposite the sides x_1 and r, respectively, leads to

$$x_1 = r\frac{\sin\theta}{\cos\beta}. \tag{A3}$$

Inserting Equations (A2) and (A3) into (A1) and rearranging gives

$$x = \left[r + (i-r)\frac{\sin\beta}{\sin\theta}\right]\frac{\sin\theta}{\cos\beta}. \tag{A4}$$

We can eliminate the angle β from this equation by noting that since twice the Bragg angle, 2θ, is the complement of the third angle of the triangle SCA whose other two angles are α and β, then

$$\beta = 2\theta - \alpha. \tag{A5}$$

Similarly, we can eliminate the angle α by applying the law of sines to the triangle SCO with the angles α and $(\pi-\theta)$ opposite the sides r and $(r+s)$, respectively, to yield

$$\sin\alpha = \frac{r}{r+s}\sin\theta = f\sin\theta, \tag{A6}$$

where we have defined

$$f = r/(r+s). \tag{A7}$$

Finally, the Bragg angle θ is related to the x-ray's wavelength λ and the energy E, as given in the main text above, by

$$\lambda = \frac{2d}{n}\sin\theta \quad \text{and} \quad E = \frac{hc}{\lambda}, \tag{A8}$$

where hc is a constant,[24] d is the lattice spacing of the crystal, and n is the order of diffraction. Substituting Equations

(A5) through (A8) into (A3), expanding the trigonometric functions using standard trigonometric identities, and defining the variable

$$u \equiv \sin\theta = \frac{nhc}{2dE}, \tag{A9}$$

gives

$$x(E) = [r + (i-r)v]\frac{u}{w}, \tag{A10}$$

where

$$v \equiv 2\sqrt{1-u^2}\sqrt{1-f^2u^2} - f(1-2u^2),$$
$$w \equiv (1-2u^2)\sqrt{1-f^2u^2} + 2fu^2\sqrt{1-u^2},$$
$$f \equiv r/(r+s), \quad u = E_0/E, \quad E_0 \equiv nhc/2d. \tag{A11}$$

This result is exact for the ideal geometry described above and applies to the general case $i \neq r$. It is not clear that this relation can be analytically inverted to give $E(x)$, but it can in any case be numerically inverted to any accuracy required. An example of the dispersion relation $E(x)$ is shown in Figure 3(a) for the spectrometer shown in Figure 1, i.e., the case of a Si(111) crystal, which has a lattice spacing of $d = 0.3136$ nm in first order ($n = 1$), curved to a radius of $r = i = 150$ mm and with the source placed $s = 210$ mm from the crystal.

While Equations (A10) and (A11) appear complex, when plotted in Figure 3(a) the smooth form of the dispersion function suggests the possibility of a simplifying approximation over limited energy ranges. Of the forms we have tested, the one that most closely matches the exact dispersion relation is

$$E^2 = \frac{a}{x^2} + b, \tag{A12}$$

where a and b are constants. Figure 3(b) plots the data in Figure 3(a) in terms of the variables E^2 and x^{-2}. The deviation from linearity is less than 1 eV. This suggests that a linear fit to calibration data plotted as E^2 against x^{-2} could provide a simple and practical spectrometer calibration scheme.

The constants a and b can be expressed in terms of the geometrical parameters of the spectrometer by the following method. Squaring both sides of Equation (A10) gives a relationship between x^2 and u^2. Note that for the spectrometers discussed in this paper, the Bragg angle is small: $\theta < 0.1$ radians for typical spectrometer parameters and $E > 22$ keV. This implies $u^2 < 0.01$ and suggests making the power series expansion of x^2 in terms of u^2 about $u^2 = 0$. This series can in turn be written in terms of E^2 using Equation (A9) above and can be inverted to give a power series for E^2 in terms of x^2 about $x^2 = 0$. The result is

$$E^2 = ax^{-2} + b + O[(x/r)^2], \tag{A13}$$

where $O[(x/r)^2]$ indicates the infinite number of additional terms of order $(x/r)^2$ and greater. The first two coefficients of the expansion are given by

$$a = E_0^2 g^2, \quad b = E_0^2 h/g, \tag{A14}$$

where

$$g \equiv r + (i-r)(2-f),$$
$$h \equiv r(2-f)^2 + (i-r)(6-8f+4f^2-f^3). \tag{A15}$$

After neglecting terms of order $(x/r)^2$ or greater one has Equation (A12) and can use this linear relation to describe the dispersion relation to acceptable accuracy where the coefficients a and b can be determined either from the physical parameters of the spectrometer using Equations (A14) and (A15) or from a linear fit to calibration data plotted as E^2 as a function of x^{-2}. This approximation provides a useful inversion of the exact dispersion relation, Equation (A10), to give E as a function of x. It can be used for initial spectrometer design and can also provide a good starting value for the numerical inversion of Equation (A10).

APPENDIX B: CRYSTAL TESTS OF RELATIVE INTEGRATED REFLECTIVITIES

The sensitivity of the curved crystal spectrometer is challenged by the common use of molybdenum filtration, the occasional use of an attenuator to compress the dynamic range of the incoming spectrum, and the reduced flux from x-ray sources at lower applied voltages. As discussed in Section IV A , this was partly offset by increasing the gain of the adc's of the image capture electronics and retrofitting the sensor with a higher sensitivity phosphor converter. In attempting to gain additional improvement in overall system sensitivity, we tested several diffraction crystals whose structure provided high reflectivity in transmission and whose mechanical properties permitted elastic bending to the required small radius without causing fracture. Our benchmark curved crystal was Si(111) with a thickness of 185 μm. Among the additional crystals investigated were Ge(111), LiF(200), abraded Si(111), heat-treated oxygen-doped Si, and Qz ($10\bar{1}1$) . The radius of bending is determined primarily by the atomic lattice spacing of the crystal and the requirement that the image be focused onto the face of the chosen detector. In this report we used a size 2 dental CCD with an active area of 36.5 mm $\times$ 25.2 mm.

It was natural to try a germanium crystal since, in flat plates, Ge provides higher integrated reflectivities than Si over the wavelength range of present interest. However, because of the lower tensile strength of Ge (in comparison with Si), the Ge had to be thinner (no thicker than 140 μm) in order to bend to a 15 cm radius of curvature without breaking. At this reduced thickness, we found Ge(111) to be less efficient in Laue (transmission) diffraction than Si(111) at 185 μm thickness. This difference was about a factor of two at 28 kV with greater disparity at lower energies. In this case, the higher absorption of Ge overcomes its higher reflectivity.

LiF(200) produced significantly brighter images than Si(111). For example, a 0.5 mm thick LiF(002) reflected about seven times more 28 keV light than a 185 μm thick Si(111). Unfortunately, the crystalline quality of commercially available LiF is poor and spectral lines are smeared.

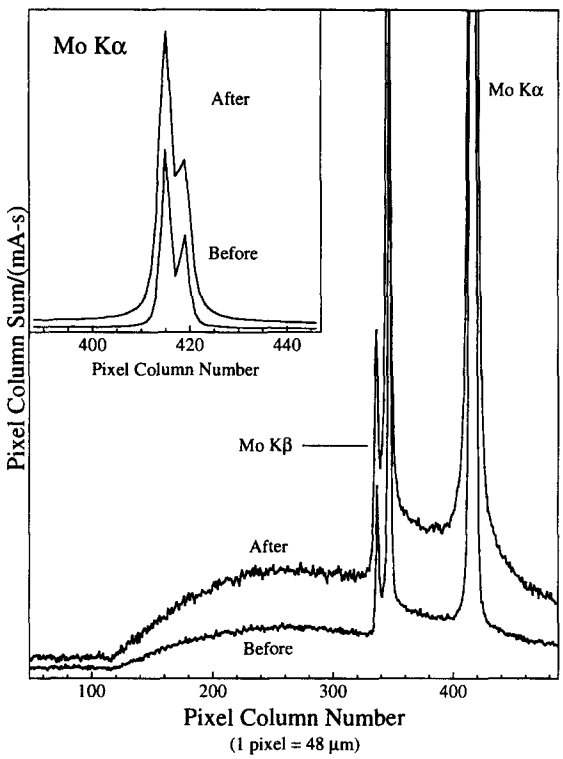

FIG. 12. The relative improvement in diffraction efficiency attained after an air-abrasive treatment of the surface of a Si crystal using the (111) planes in transmission.

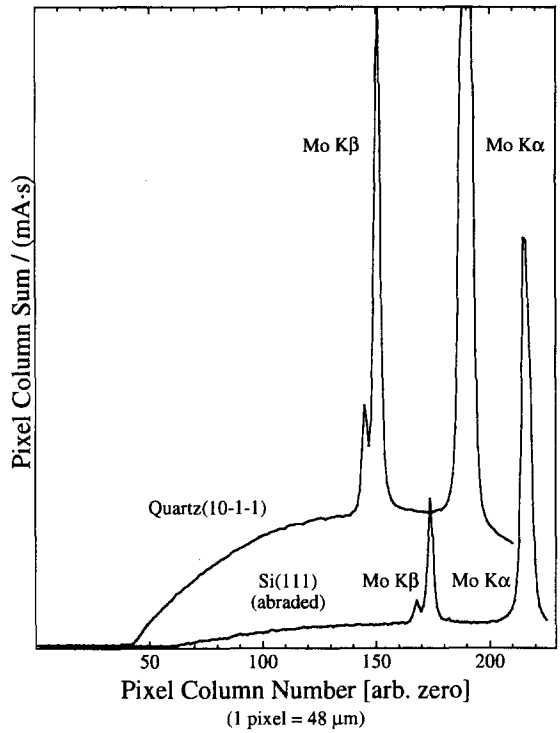

FIG. 13. Comparison of spectra acquired from an abraded Si(111) crystal (0.185 mm thickness) and a Qz ($10\bar{1}1$) crystal (0.25 mm thickness).

X-ray topography revealed multiple domains in our fusion-grown LiF crystal. The lattice spacing of LiF(200) would also require a heat-treatment to bend LiF to the 10.2 cm radius of curvature required to focus the image onto the presently used dental sensor without fracturing the crystal.

The narrow diffraction widths (~1 to 2 eV) of perfect crystals imply a considerable loss in x-ray sensitivity relative to a more optimally matched width (~100 eV) required in the present application. We tried, therefore, by various means to introduce a gradient in the crystal's interplanar spacing to increase the acceptance bandwidth and hence the instrument's efficiency. First we attempted to introduce a strain gradient near the surface of a silicon crystal by rouge polishing. This proved ineffective. In marked contrast, the application of an air abrasive treatment using fine aluminum oxide grit produced an energy-dependent increase of throughput—about a factor of two at 28 keV. This enhancement was quickly brought to saturation after a frosted appearance was produced on the surface; the effect was easily reproduced on other Si crystals. Spectra from before and after this surface abrasion treatment are shown in Figure 12. The lower two spectra show the enhancement of Bremsstrahlung intensity between Mo Kβ (19.6 keV) and the endpoint energy of 33 kV. The inset spectra show the enhancement of intensity at Mo Kα (17.5 keV) and the concomitant loss of resolution. These data were acquired with a CCD dental sensor that had not been retrofitted with a thicker scintillating screen and hence still exhibit resolved Kβ emissions of Mo.

We also tested analyzing crystals of Si(111) which possessed defects distributed throughout the bulk[30] and so might be expected to exhibit even further enhanced throughput. These samples were cut from silicon which had been grown by the Czochralski technique and so contained an incorporated oxygen concentration of about 10^{18} atoms·cm^{-3}. The bulk defects are created by annealing at temperatures above 550 °C which causes oxygen to precipitate as a form of silica. After annealing, great enhancements in the integrated reflectivity have been observed at 317 keV.[30] The integrated reflectivity at the lower energies used in the present application, however, is less sensitive to the creation of a relatively small mosaic spread; the results were comparable to that of untreated silicon at the resolution of the dental CCD.

Our present prototype spectrometers use quartz (SiO_2) analyzing crystals. The brightest peak in the quartz x-ray powder pattern is designated as 101. Contributing to this peak are two differently oriented sets of diffraction planes with the same atomic spacing of 0.3343 nm. Calculations from the code of Brennan and Cowan[30] predicted that the ($10\bar{1}1$) or so-called minor planes (also known as the z planes of quartz) would exhibit about a 50% higher reflectivity than the ($10\bar{1}1$) major planes (also known as the r planes) at Mo Kα. Our supplier provided polished crystals of natural Brazilian quartz cut to the dimensions 47.0 mm ×27.5 mm ×0.23 mm. (Valpey-Fisher Corporation, Hopkinton, MA.) The Qz ($10\bar{1}1$) diffraction planes gave the highest reflectivity among the crystals tested. The spectra from Qz ($10\bar{1}1$) and abraded Si(111) which are compared in Figure 13 were acquired under identical experimental conditions: 30 kV applied to a small focus Mo x-ray tube without added filtration

for an exposure of about 20 mAs. Both crystals were bent to a radius of curvature of 15 cm. Since the reflecting planes used in the two crystals have slightly different atomic spacings, the energy scale of the two spectra is different; they have been offset along the abscissa axis to show the region near the endpoint energies. A dark image has been subtracted in both cases before computing the column sum; the spectra are plotted on the same ordinate scale without offset. The Mo Kα emission saturates the CCD in the spectrum from quartz.

The data reveal that the diffraction efficiency from the quartz crystal used is about a factor of four to five greater than that from the abraded silicon crystal. Since the gain due to abrading the silicon crystal was up to a factor of two (Figure 12), there is a net enhancement of about a factor of eight between the two materials oriented as described. We measured the transmission rocking curves of these two materials in the form of flat plates at these given thicknesses and found their reflectivity at Cu Kα to be comparable. This result is in accord with the calculations of dynamical diffraction theory.[31] One contributing factor to the higher intensity in the spectrum recorded using bent quartz over that of bent silicon is that the tensile strength of quartz considerably exceeds that of Si, permitting the use of thicker crystals; in this case the quartz crystal is 250 μm thick while the silicon is 185 μm thick. But the primary cause is due to the so-called Sumbaev effect,[29] which is known to be particularly pronounced in quartz. The enhancement arises from the behavior of the planes normal to the surface as the crystal is cylindrically bent. These reflecting planes elastically take the form of parabolic surfaces, producing a quasimosaic effect which significantly broadens the rocking curve; additionally it causes slightly different relative reflectivities for the two "mirror" spectra registered. Cut for transmission, bent Si(111) does not exhibit the Sumbaev effect; our quartz crystals were cut with a tip angle such that this effect is near maximum. These aspects of x-ray diffraction in quartz emerge quite naturally from a more general treatment of x-ray diffraction in such structurally and elastically anisotropic crystals.[32]

[a]Present address: School of Physics, University of Melbourne, Parkville, Victoria 3052 Australia.

[1]See, for example *Syllabus: A Categorical Course in Physics Technical Aspects of Breast Imaging*, edited by A. G. Haus and M. J. Jaffe (Radiological Society of North America, Oak Brook, IL, 1992).

[2]J. Law, K. Faulkner, and S. Smith, "Variation of image quality with x-ray tube potential in mammography," Br. J. Radiol. **62**, 192–194 (1989).

[3]J. Law, "The measurement and routine checking of mammography x-ray tube kV," Phys. Med. Biol. **36**, 1133–1139 (1991).

[4]M. Misakian, "High voltage divider and resistor calibration," NBS Technical Note 1215 (July 1985), available from Superintendent of Documents, U.S. Government Printing Office, Washington, DC 20402.

[5]G. Hein, P. Pychlau, and E. Schüle, "NOMEX-A universal diagnostic dosemeter, mA·s, and kV meter for acceptance test measurements and quality assurance," Radiat. Protect. Dosimetry **43**, 187–191 (1992).

[6]W. E. Simon and D. Richards, "Determination of x-ray tube potential (kV) wave form by a noninvasive evaluation of radiation output (NERO)," SPIE **273**, 149–152 (1981),

[7]W. E. Simon, "Noninvasive evaluation of a diagnostic x-ray machine using the Victoreen Model 6000A NERO," Br. J. Rad. Suppl. **18**, 96–99 (1985).

[8]J. R. Greening, "The measurement by ionizing methods of the peak kilovoltage across x-ray tubes," Br. J. Appl. Phys. **6**, 73–78 (1955).

[9]T. R. Fewell and K. E. Weaver, "The measurement of diagnostic x-ray spectra with a high purity germanium spectrometer," SPIE **56**, 9–18 (1975).

[10]G. Matscheko and R. Ribberfors, "A Compton scattering spectrometer for determining xray photon energy spectra," Phys. Med. Biol. **32**, 577–594 (1987).

[11]G. Matscheko and R. Ribberfors, "A generalised algorithm for spectral reconstruction in Compton spectroscopy with corrections for coherent scattering," Phys. Med. Biol. **34**, 835–841 (1989).

[12]G. A. Carlsson, K. Berggren, C. A. Carlsson, G. Matscheko and R. Ribberfors, "The Compton spectrometer," Int. J. Quantum. Chem. **35**, 721–734 (1989).

[13]L. Stanton, D. A. Lightfoot, and S. Mann, "A penetrameter method for field kV calibration of diagnostic x-ray machines," Radiology **87**, 87–98 (1966).

[14]G. M. Ardran and H. E. Crooks, "Checking diagnostic x-ray beam quality," Br. J. Radiol. **41**, 193–198 (1968).

[15]A. F. Jacobson, J. R. Cameron, M. P. Siedband, and J. Wagner, "Test cassette for measuring peak tube potential of diagnostic x-ray machines, Med. Phys. **3**, 19–25 (1976).

[16]T. E. Sheridan, "Apparatus for measuring the peak voltage applied to a radiation source," U.S. Patent No. 4843619, June 27, 1989, assigned to Kiethley Instruments, Inc.

[17]M. Davison and J. Law, "Measurement of the voltage of diagnostic x-ray tubes using K-characteristic fluorescence," Phys. Med. Biol. **17**, 572–576 (1972).

[18]R. D. Deslattes, J. C. Levin, M. D. Walker, and A. Henins, "Noninvasive high voltage measurement in mammography by crystal diffraction spectrometry," Med. Phys. **21**, 123–126 (1994).

[19]E. Rutherford and E. N. da C. Andrade, "The spectrum of the penetrating γ-rays from Radium B and Radium C," Philos. Mag. **28**, 263–273 (1914).

[20]E. Rutherford and E. N. da C. Andrade, "The wavelength of the soft γ-rays from Radium B," **17**, 854–868 (1914).

[21]R. D. Deslattes, U.S. Patent No. 5,381,458, June 10, 1995, assigned to NIST, currently licensed to Radcal Corporation, Monrovia, CA.

[22]Y. Cauchois, "Spectrographie des rayons x par transmission d'un faisceau non canalisé a travers un cristal courbé (I)," J. Phys. Rad. **3**, 320–336 (1932).

[23]C. T. Chantler, R. D. Deslattes, A. Henins, and L. T. Hudson, "Flat and curved crystal spectrography for mammographic x-ray sources," Br. J. Radiol. **69**, 636–649 (1996).

[24]E. R. Cohen and B. N. Taylor, "The 1986 adjustment of the fundamental physical constants," CODATA Bulletin **63** (Pergamon, Elmsford, NY, 1986) pp. 1–32.

[25]J. D. Cox, D. S. Langford, and D. W. Williams, "Electronic intraoral dental x-ray imaging system employing a direct sensing CCD array," SPIE Vol. 2009 X-Ray Detector Physics and Applications II, 1993, pp. 36–47.

[26]J. Janesick and T. Elliott, "History and advancements of large area array scientific CCD imagers," ASP Conf. Ser. **23**, 1–67 (1992).

[27]C. Kimme-Smith, L. W. Bassett, and R. H. Gold, "Focal spot size measurements with pinhole and slit for microfocus mammography units," Med. Phys. **15**, 298–303 (1988).

[28]See for example, C. T. Chantler, "Theoretical form factor, attenuation, and scattering tabulation for $Z=1-92$ from $E=1-10$ eV to $E=0.4-1.0$ MeV," J. Phys. Chem. Ref. Data **24**, 71–643 (1995).

[29]O. I. Sumbaev, "Experimental investigation of the elastic quasi-mosaic effect," Sov. Phys. JETP **27**, 724–728 (1968).

[30]J. R. Schneider, O. D. Conçalves, A. J. Rollason, U. Bonse, J. Lauer, and W. Zulehner, "Annealed Czochralski grown silicon crystals: A new material for the monochromatisation of synchrotron radiation and x-rays above 60 keV," Nucl. Instrum. Methods B **29**, 661–674 (1988).

[31]S. Brennan and P. L. Cowan, "A suite of programs for calculating x-ray absorption, reflection, and diffraction performance for a variety of materials at arbitrary wavelengths," Rev. Sci. Instrum. **63**, 850–853 (1992).

[32]In particular, the magnitude of the enhanced reflectivity of the (10-1-1) planes of curved quartz crystals in a transmission geometry is in agreement with that predicted by the dynamical diffraction calculations of J. H. Marshall, Radcal Corporation, Monrovia, CA (private communication).